ELSEVIER

Polymer 40 (1999) 4795–4803

polymer

Stratification in thermoplastic olefins (TPO); photoacoustic FT-IR depth profiling studies

B.D. Pennington[a], R.A. Ryntz[b], M.W. Urban[a,*]

[a]*Department of Polymers and Coatings, North Dakota State University, Fargo, ND 58105, USA*
[b]*Automotive Components Division, Ford Motor Company, Dearborn, MI 48121, USA*

Received 19 May 1998; received in revised form 17 September 1998; accepted 24 September 1998

Abstract

Photoacoustic Fourier Transform infrared (PA FT-IR) depth profiling experiments ranging from 3 to 50 μm into the surface of thermoplastic olefin (TPO) show that the crystalline polypropylene (PP) phase resides at approximately 7–9 μm below the TPO surface, while ethylene-polypropylene rubber (EPR) layer is present at 15 μm, and extends into the bulk. In an effort to determine the distribution of PP and EPR components, a calibration method was developed by ratioing pure PP and EPR bands at 2953 and 2849 cm^{-1} at 10/90, 25/75, 50/50, 75/25, and 90/10 ratios. Comparison of this numerical data and the experimental results allows determination of the distribution of EPR and PP components across the film thickness. It appears that the EPR region is predominantly present at 15 μm below the surface, while PP is located at shallower depths. Concentration variations of talc can be also followed by monitoring the band at 1019 cm^{-1} caused by Si–O stretching modes and its content is higher near the TPO surface. Based on these studies, a stratification model for TPO is proposed.

Keywords: Photoacoustic FT–IR surface depth profiling; Thermoplastic olefins; Surface stratification

1. Introduction

Thermoplastic olefin (TPO) is a rubber-toughened polymer blend of polypropylene (PP), ethylene propylene rubber (EPR), polyethylene (PE), pigments, fillers, and additives. Owing to low density, durability, and thermoplastic physical properties, polypropylene is the major component of TPO. While addition of EPR provides low temperature impact strength, incorporation of pigments, fillers, thermal antioxidants, plasticizers, and processing aids, improve mechanical strength, performance and processability [1]. As the distribution of individual TPO components may have significant effects on such properties as adhesion, durability, and other surface related properties, understanding of the distribution of individual components is particularly important. As a matter of fact, the phenomena of stratification of various components in organic coating has been observed spectroscopically on numerous systems, including melamine-polyester [2], alkyds [3], urethanes [4–6], and latexes [7–17], just to name a few.

Previous studies on polypropylene blend properties concentrated on polymer composition [18], processing conditions [19], morphology [20], mechanical response [21], and paintability [22]. These studies have shown that a relatively small change in processing will have a drastic response on final properties [23,24]. While the effect of compression molding on polypropylene/EPR rubber blends has been addressed [25], injection molding introduces other variables which influence polymer morphology.

In this study, we will examine how processing will affect the distribution of individual components in TPO. To achieve this objective, we will utilize photoacoustic Fourier Transform infrared (PA FT-IR) spectroscopy, in particular, its nondestructive capability of surface depth profiling.

2. Experimental

2.1. Materials

TPO was obtained from Ford Motor Co. as an injection-molded plaque of 3.8 mm thickness. Isotactic polypropylene (Ford Motor Company) was obtained in a 2.5 mm diameter pellet form at 46% crystallinity. EPR was received from Ford Motor Company in a molded sheet form 5 mm thick and contained a primary antioxidant to prevent thermal oxidation. Magnesium silicate (talc, $3MgO{\cdot}4SiO_2{\cdot}H_2O$;

* Corresponding author. Tel.: +1-701-231-7633; fax: +1-701-231-8439.
E-mail address: urban@plains.nodak.edu (M.W. Urban)

0032-3861/99/$ - see front matter
PII: S0032-3861(98)00714-9

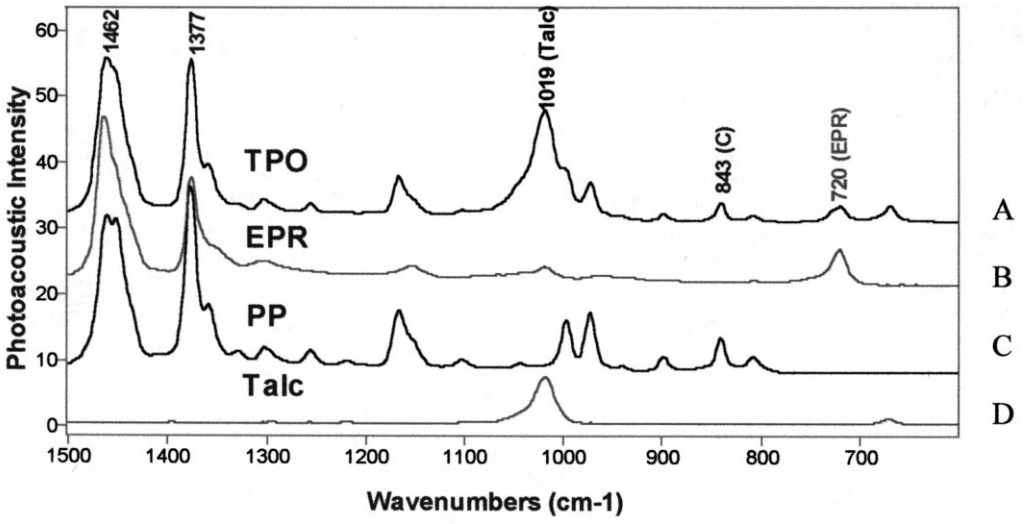

Fig. 1. Photoacoustic FT-IR spectra of: TPO (Trace A); EPR (Trace B); PP (Trace C) components collected at a mirror velocity of 0.16 cm/s for penetration depths of 10 to 16 μm over the spectral range 1500 to 600 cm^{-1}.

Mallinckrodt) was obtained as a powder and used as a reference standard for photoacoustic analysis.

2.2. Analytical measurements

Linear rapid-scan mode PA FT-IR spectra were collected on a Nicolet Magna-IR 850 FT-IR spectrometer equipped with a MTEC Model 100 photoacoustic cell designed for condensed phase sample analysis. Surface depth profiling analysis was achieved by varying the interferometer mirror velocity (V) which dictates the modulation frequency (ω) of the infrared radiation [26,27]. These quantities are related by the following equation:

$$\omega = 2\bar{\nu}V \tag{1}$$

where: $\bar{\nu}$ is the spectral wavenumber [28,29]. For optically opaque and thermally thick specimens, such as TPO, the sampling depth can be estimated using the relationship between optical absorption and thermal diffusion lengths. The optical absorption length, l_β, is the distance the IR light will be attenuated by a factor of e^{-1}, and the thermal diffusion length, μ_{th}, is defined as the distance in which the resultant thermal wave is damped by the same factor. Owing to the sample dimensions, the sample thickness is much greater than either l_β or μ_{th}. For optically opaque and thermally thick specimens ($6l_\beta > \mu_{th}$), the depth of penetration can be expressed by the following equation [30,31].

$$\mu_{th} = \left(\frac{2\alpha}{\pi\omega}\right)^{1/2} \tag{2}$$

where: α is the thermal diffusivity (cm^2/s) is expressed as $\kappa/\rho C$, where κ is the thermal conductivity, ρ is the density, and C is the specific heat. According to Eq. (2), the thermal diffusion length is inversely proportional to the modulation frequency ω, assuming that full saturation conditions are avoided, as would be the case for $2\pi l_\beta > \mu_{th}$. Under these conditions, the depth of penetration will not be accurately reflected by Eq. (2) since the IR light will be completely damped at $2\pi l_\beta$ and will not penetrate to the thermal diffusion length depth. Therefore, the relative content of the functional groups that absorb IR radiation at specific depths can be determined by changing ω, thus facilitating depth profiling experiments. Modulation frequencies employed in these experiments were $1.9\bar{\nu}$, $1.3\bar{\nu}$, $0.95\bar{\nu}$, $0.64\bar{\nu}$, $0.32\bar{\nu}$, $0.13\bar{\nu}$, $0.094\bar{\nu}$, $0.064\bar{\nu}$, and $0.032\bar{\nu}$ Hz, allowing approximate depths of penetration from 3 to 50 μm into the surface. The following κ, ρ, and Cp values were used: 0.0012 W/cm·K, 0.91 g/cm^3, and 1.79 J/K·g, respectively. Using these values, the thermal diffusivity was determined to be 7.4×10^{-4} cm^2/s. Following data acquisition, the interferogram was ratioed to a carbon black reference, with further spectral processing accomplished using Nicolet Omnic and Galactic Industries Grams/32 software. It should be noted that the limit of depth resolution varies with the depth of penetration; for example, when modulation frequency is changed from $1.9\bar{\nu}$ to $1.6\bar{\nu}$, the penetration depth changes from approximately 3 to 3.4 μm. However, for slower modulation frequencies this difference will be higher, ultimately leading to a lower spatial resolution. Our recent experiments show that one can obtain a significant enhancement of spatial resolution using a step-scan mode as well as phase rotational analysis [32].

Dynamic mechanical thermal analysis measurements were conducted on a Rheometrics Mark III at a frequency of 10 Hz and a force of 0.02 N. The sample was measured in the tensile mode, recording the storage modulus, loss modulus, and tan δ at a heating rate of 10°C/min.

3. Results and discussion

One of the factors that may significantly influence surface

Table 1
IR active bands of thermoplastic olefin (TPO), polypropylene (PP), ethylene propylene rubber (EPR) elastomer and talc [33,50,51]

TPO (cm^{-1})	PP (cm^{-1})	EPR (cm^{-1})	Talc (cm^{-1})	Assignment
			3675	OH stretch (free)
2953	2954	2947		CH_3 asym stretch
2922	2920	2925		CH_2 asym stretch
2870	2877			CH_3 sym stretch
2849	2838	2853		CH_2 sym stretch
2723				CH_2 asym bend
			1669	OH bend
1462	1458	1463		CH_3 asym bend
1453				CH_2 bend + CH_3 asym bed
1377	1376	1376		CH_3 sym bend + CH_2 wag + C–C chain stretch
1360	1358			CH bend + C–C chain stretch + CH_2 wag + CH_3 sym bend
1304	1304			CH_2 wag + CH_2 twist + CH bend
1257	1261			CH bend + CH_2 twist + CH_3 rock
1166	1168			C–C chain stretch + CH_3 rock + CH bend
	1045			C–CH_3 stretch + C–C chain stretch + CH bend
			1027	Si–O stretch
			1019	Si–O stretch
1000	999			CH_3 rock + CH_2 wag + CH bend
973	972			CH_3 rock + C–C chain stretch
843	841			CH_2 rock + C–CH_3 stretch
	806			CH_2 rock + C–C chain stretch + CH bend
		720		CH rocking
	455			C–C–C bend

composition of a substrate in the direction normal to the surface are stratification processes of individual components. This issue is particularly important for multi-component systems, such as TPO, as individual components may stratify at different rates and their concentration levels may vary as a function of distance from the surface. As a first step in the analysis of component distribution across the TPO substrate, it is necessary to assign IR bands to individual components. Fig. 1 illustrates PA FT-IR spectra of TPO (Trace A) in the 1500 and 600 cm^{-1} region and its major individual components of TPO: EPR (Trace B), PP (Trace C), and talc (Trace D). Fig. 1, Trace A, shows RPA FT-IR spectrum of TPO with the bands at 1462 cm^{-1} caused by CH_3 asymmetric bending vibrations and the band at 1377 cm^{-1} caused by CH_3 symmetric bending, CH_2 wagging, and C–C chain stretching vibrations. The band at 1019 cm^{-1} results from Si–O stretching vibrations of talc. The crystalline content of TPO can be identified by monitoring the bands at 1000 and 843 cm^{-1} owing to PP crystalline phase [33]. The 1000 cm^{-1} band is attributed to

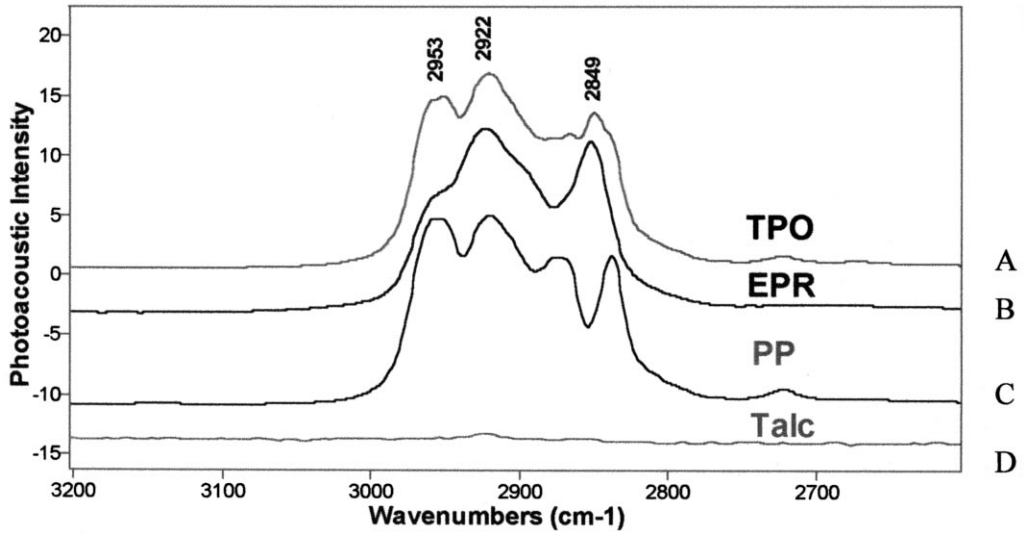

Fig. 2. Photoacoustic FT-IR spectra of TPO (Trace A); EPR (Trace B); PP (Trace C) components collected at a mirror velocity of 0.16 cm/s for penetration depths of 7 to 8 μm over the spectral range 3200 to 2600 cm^{-1}.

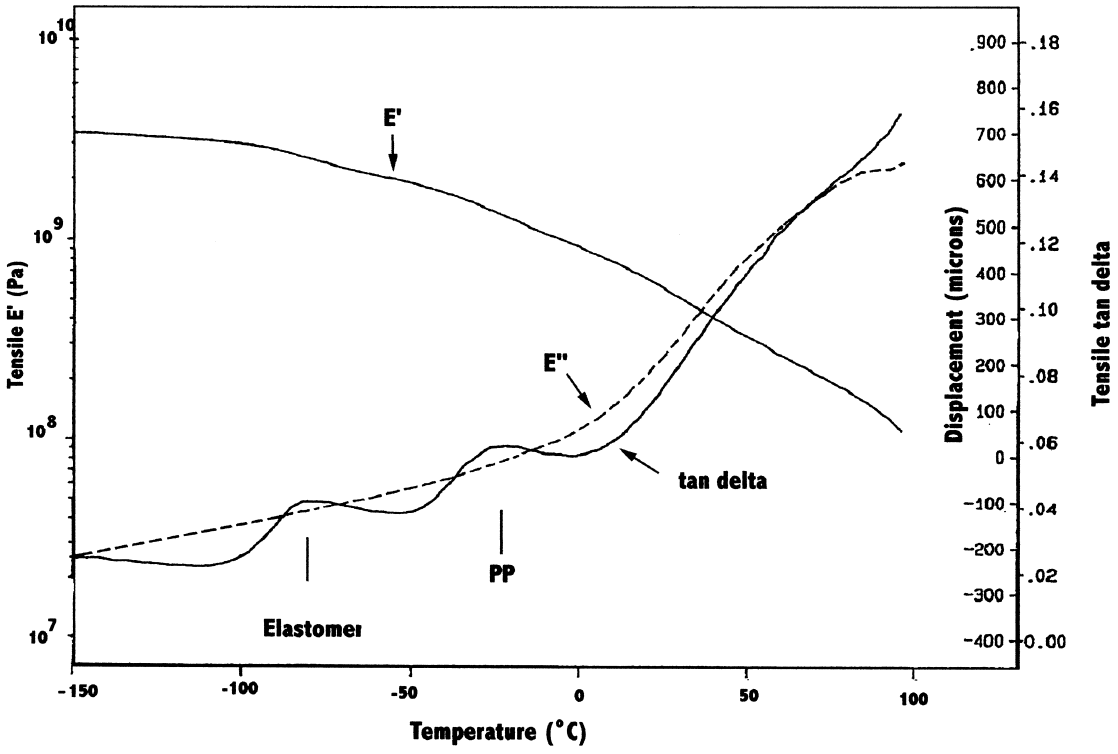

Fig. 3. Dynamic mechanical thermal analysis (DMTA) of TPO collected every 4 s as the temperature was varied from − 150°C to 100°C at 10.0°C per minute at a frequency of 10 Hz and a force of 0.02 N. Shown are the transitions illustrating the phase separation of the PP and EPR regions.

the combination of CH_3 rocking, CH_2 wagging, and CH bending motions, while the 843 cm^{-1} represents the coupled CH_3/CH deformation and CH_2/CH_3 rocking normal vibrations [34]. The band at 720 cm^{-1} results from CH rocking modes of ethylene groups in EPR. As the EPR is a cross-linked network made up of similar entities as polypropylene, similar bands are detected in PP and EPR. Table 1 lists observed IR bands of each component and their tentative assignments.

Another spectral region of interest, which is shown in Fig. 2, is the 3200–2600 cm^{-1} region. The bands at 2953, 2922, and 2849 cm^{-1} are the result of the CH stretching vibrations of the CH_3 asymmetric, CH_2 asymmetric, and CH_2 symmetric stretching modes, respectively. Although the overlap of the bands as a result of EPR (Trace B) and PP (Trace C) may make interpretation of the TPO spectrum (Trace A) difficult, this region is quite useful because the band at 2849 cm^{-1} is sensitive to the presence of EPR, while the band at 2953 cm^{-1} is responsible for the PP phase.

In an effort to set the stage for spectroscopic surface depth profiling analysis, let us first consider the results of dynamic mechanical thermal analysis (DMTA). It is well known that this experimental approach is a commonly accepted method that can provide information about phase separation in multi-component systems [35,36]. Previous studies on latexes [37] and other polymers [38] using DMTA have shown that the phase separation of a two component system is represented by the occurrence of two glass transition temperatures (Tg). In the case of TPO, the tan δ curve shown in Fig. 3 contains two maxima at −80 and −25°C, corresponding to Tg's of EPR and PP, respectively [39]. If TPO was homogeneous, one would expect a single broader maximum. This data indicates that the phase separation between EPR and PP does occur, but no information as to the spatial distribution of these components can be obtained. For that reason, we will employ PA FT-IR spectroscopy.

While previous studies have [2–17] shown changes in component distribution across the sample thickness, the methods used to characterize these changes are destructive. As a result of that, they may alter original specimen morphology; for example, crystallization may be induced from the shear forces encountered in microtoming. As a matter of fact, it has been shown that artificial crystalline morphology is generated by oxidative stresses during sample preparation techniques [20]. Sample preparation may also change the anticipated depth of analysis from compression or deformation of the sample [18]. For that reason, this study focuses on the use of surface depth profiling using PA FT-IR spectroscopy, since this approach offers nondestructive surface analysis, and thus more accurate determination of the distribution of individual components across the film thickness can be obtained.

Fig. 4 illustrates a series of PA FT-IR spectra recorded at modulation frequencies of $1.9\bar{\nu}$ to $0.032\bar{\nu}$ at 1500 to 600 cm^{-1} which allows surface depth profiling from deeper

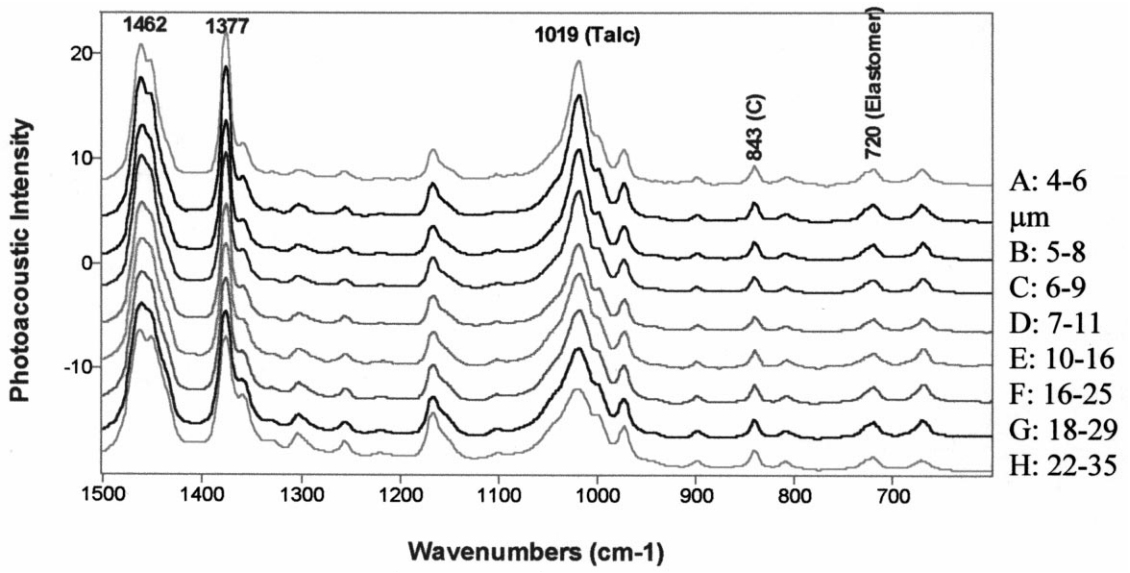

Fig. 4. Photoacoustic FT-IR analysis for penetration depths of 4 to 50 μm (Traces A-I) for thermoplastic olefin (TPO) over the spectral range 1500 to 600 cm^{-1}.

regions below the surface, approximately 4 to 50 μm. Integration of the band at 843 cm^{-1} as a result of crystalline PP phase shows the largest photoacoustic response at 7–9 μm below the surface from the spectra recorded as Traces B, C, and D. Below 9 μm, this band gradually diminishes while going into the bulk. The EPR elastomer band at 720 cm^{-1} increases at the modulation frequency of 230 Hz. This spectral response indicates an increase of the CH rocking vibrational modes of ethylene units in EPR at an approximate penetration depth of 15 μm. These observations agree with the previous studies which showed that injection molding of EPR/PP blends will result in stratifying of the rubbery region below the surface [40]. However, the spectroscopic analysis presented above extends the scope of previous findings indicating that concentrations of PP and EPR components of TPO vary between 5 and 15 μm, with the EPR layer lying below the PP region.

To further advance how PP and EPR distribution varies near the TPO surface, we will take advantage of the linear PAS wavenumber dependence on the depth of penetration. For that reason, we will focus on the C–H stretching region of TPO between 3200 and 2600 cm^{-1} where, owing to the

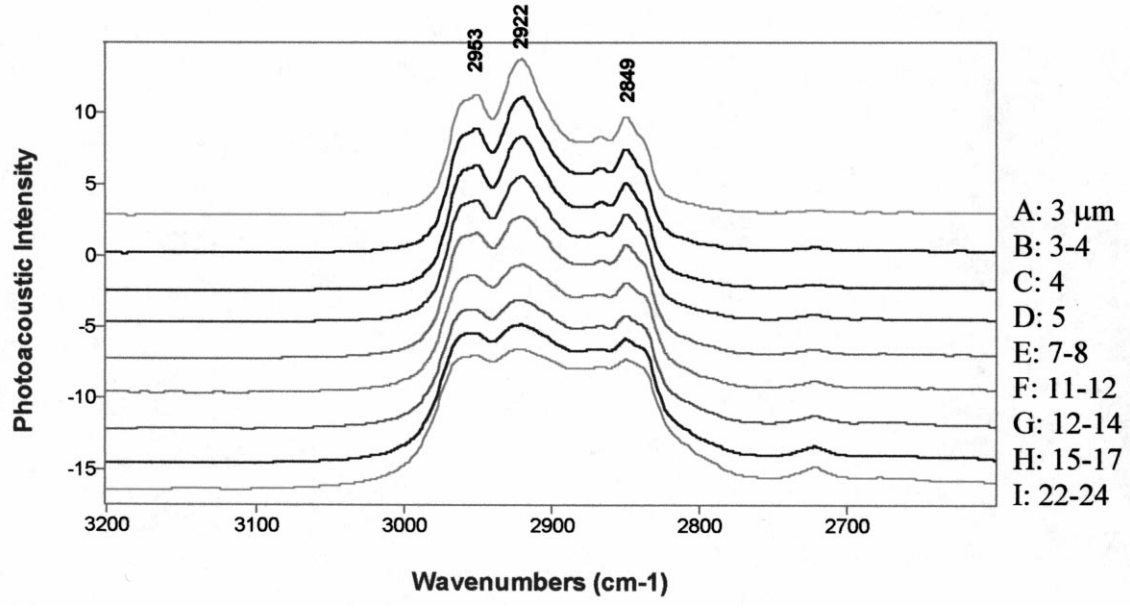

Fig. 5. Photoacoustic FT-IR analysis for penetration depths of 3 to 24 μm (Traces A-I) for thermoplastic olefin (TPO) over the spectral range 3200 to 2600 cm^{-1}.

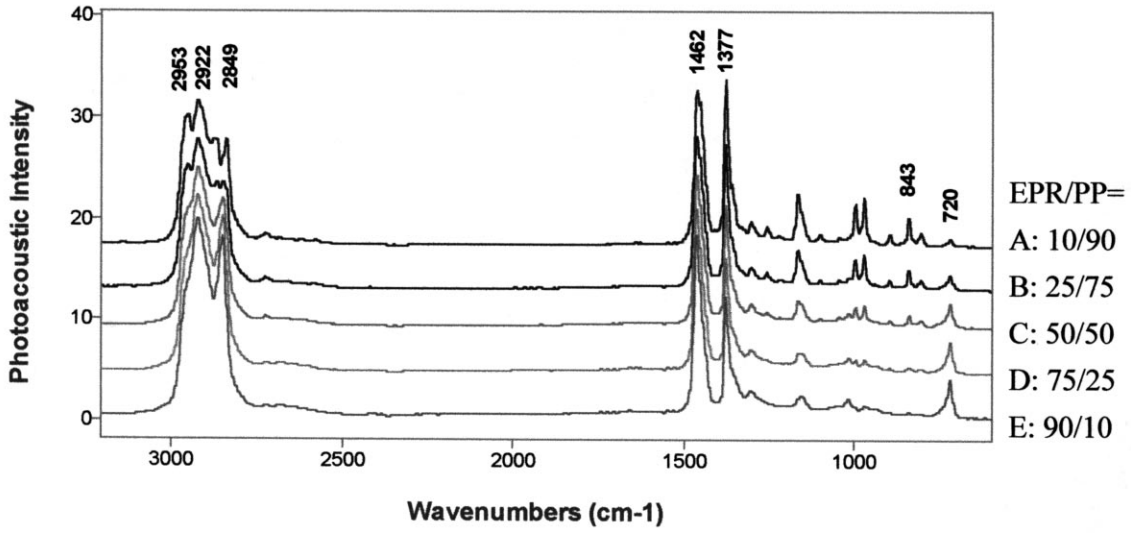

Fig. 6. Numerical spectra of polypropylene and elastomer components at ratios of 10/90 (Trace A), 25/75 (Trace B), 50/50 (Trace C), 75/25 (Trace D), 90/10 (Trace E) in the spectral range 3200 to 600 cm^{-1}.

wavenumber dependence, shallower depths of penetration are achieved. Fig. 5 illustrates PA FT-IR spectra of TPO recorded with modulation frequencies of $1.9\bar{\nu}$ to $0.032\bar{\nu}$ Hz which allows us to observe the response from 3 to 24 μm. All spectra were normalized to the band at 1377 cm^{-1} owing to a combination band resulting from CH_3 symmetric bending, CH_2 wagging, and C–C chain stretching normal vibrations. As shown, the 2849 cm^{-1} band increases with the increasing penetration depth. As the response of the 2849 cm^{-1} band is significantly greater for EPR than for PP, Fig. 5 demonstrates that EPR lies deeper into the surface than PP. As the 2953 cm^{-1} band is stronger than the 2849 cm^{-1} band at 3 μm (Trace A) than at 23 μm (Trace I), the region nearer the surface is richer in PP.

As indicated earlier, this spectral region represents several overlapping bands, but it can be quite useful as it may allow us to obtain individual component information. As it is practically impossible to obtain TPO specimens with specific concentrations of individual components at specific depths from the surface, we will create numerical spectra out of the pure EPR and PP component spectra. This approach not only allows us to interpret the depth profiling data, but also eliminates possible interfacial interactions between PP and EPR in a blended system. Numerically generated spectra for EPR and PP at ratios of 10/90 (Trace A), 25/75 (Trace B), 50/50 (Trace C), 75/25 (Trace D), and 90/10 (Trace E) are shown over the 3200 to 600 cm^{-1} spectral range in Fig. 6. Normalization to the 1377 cm^{-1} band allows us to monitor the presence and distribution of EPR with respect to PP by monitoring the intensity changes of the bands at 2953 and 2849 cm^{-1}. As expected, the band at 2953 cm^{-1} in Fig. 6 decreases as the amount of PP decreases. At the same time, the 2849 cm^{-1} band increases, indicating an increase in the EPR content. In addition, the 720 cm^{-1} band increases owing to the increased amount of EPR, while the 843 cm^{-1} response of PP decreases for a higher EPR/PP ratio. This data confirms the previous interpretation of the spectra shown in Fig. 4, where higher EPR content is detected at 15 μm from the surface. These results also agree with the studies by Ramamurthy and Ryntz [1], in which DSC analysis of microtomed sections of TPO showed higher content of polypropylene in the 10 μm below the TPO surface.

In an effort to interpret the spectra of TPO recorded from various depths (Figs. 4 and 5), we will use the band ratio 2953/2849 cm^{-1} of the computer generated spectra (Fig. 6), and compare with the experimental results (Fig. 5). This is shown in Fig. 7. The computer data, shown by curve A of Fig. 7, reflect the ratio of mathematically combined spectra of EPR and PP and demonstrates that, as the elastomer component increases, a linear decrease of the 2953/2849 ratio occurs. The experimental data shown by curve B of Fig. 7 displays the intensity ratio of the bands at 2953 cm^{-1} and 2849 cm^{-1}, but an exponential decrease is observed while going from the surface to the bulk of TPO. This observation indicates that a higher content of PP exists near the surface, and decreases nonlinearly into the bulk. As the new spectral features are not detected, it is believed that no interactions among individual components are detected. At 15 μm below the surface, the 2953/2849 ratio levels off to approach unity, indicating a decrease of PP and no further stratification. The exponential dependence of the 2953/2849 ratio demonstrates a non-homogeneous distribution in this blended system, thus confirming the assessment of data in Fig. 4, which showed that EPR stratifies at approximately 15 μm. The indication of non-homogeneous distribution of the EPR and PP components is confirmed by the DMTA measurements shown in Fig. 3. It should be noted that, in spite of the fact that DMTA is commonly used to identify phase separations in polymeric systems, it

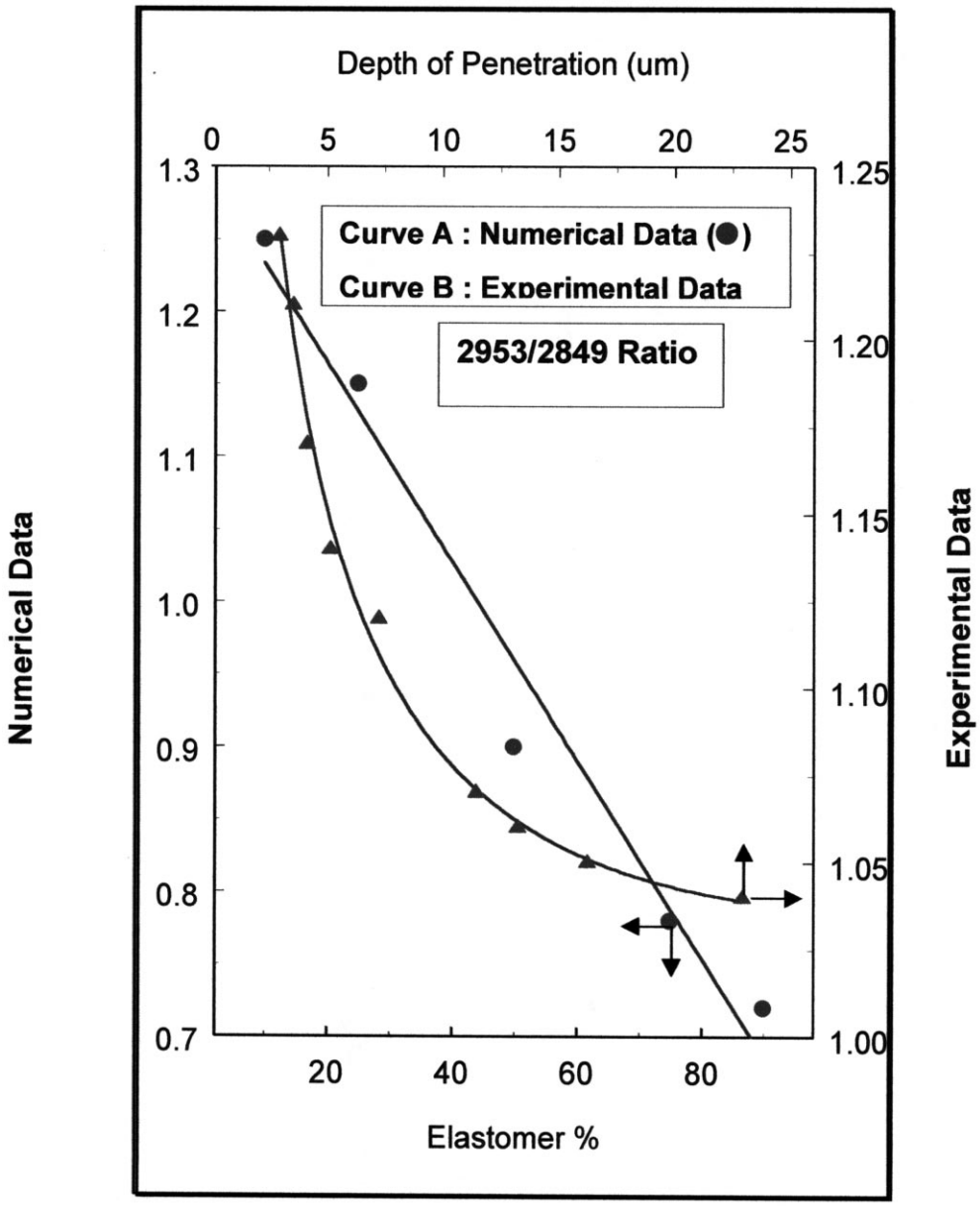

Fig. 7. Photoacoustic intensity ratio of 2953 and 2849 cm^{-1} bands normalized to 1377 cm^{-1} for numerical (Trace A) and experimental (Trace B) spectra of thermoplastic olefin (TPO).

is not capable of spatial determination of component distribution.

Photoacoustic analysis can also be used to follow the presence and stratification of talc. As illustrated in Fig. 4, the intensity changes of the 1019 cm^{-1} band decreases as the depth of penetration increases. Analysis of Traces A through C indicates that the highest content of talc lies predominantly 5 to 7 μm below the surface, and its concentration diminishes while going into the bulk. As the presence of crystalline PP accompanies the presence of talc, there is likely to be a nucleating effect of molten PP in the presence of talc. Previous studies have shown that the talc component will have an affinity for the PP crystalline region [41].

Previous studies have shown that the injection molding of TPO results in stratification of individual components as a result of shear, flow, and thermal processes [42]. According to the literature [22,43], the primary parameters that may affect TPO morphology are temperature of the mold, injection time and pressure, and cooling rates. As a polymer melt is allowed to cool against a high energy surface, such as a metal, the polymer surface will nucleate rapidly, often normal to the surface [44]. Under injection molding conditions, TPO will form a ''skin'' at the surface which is composed of high density, nonspherulitic polypropylene structures having a slight degree of orientation of polymer chains in the flow direction [45,46]. The skin formation results from the rapid decrease of temperature as the polymer melt contacts the cooler mold surface that causes rapid

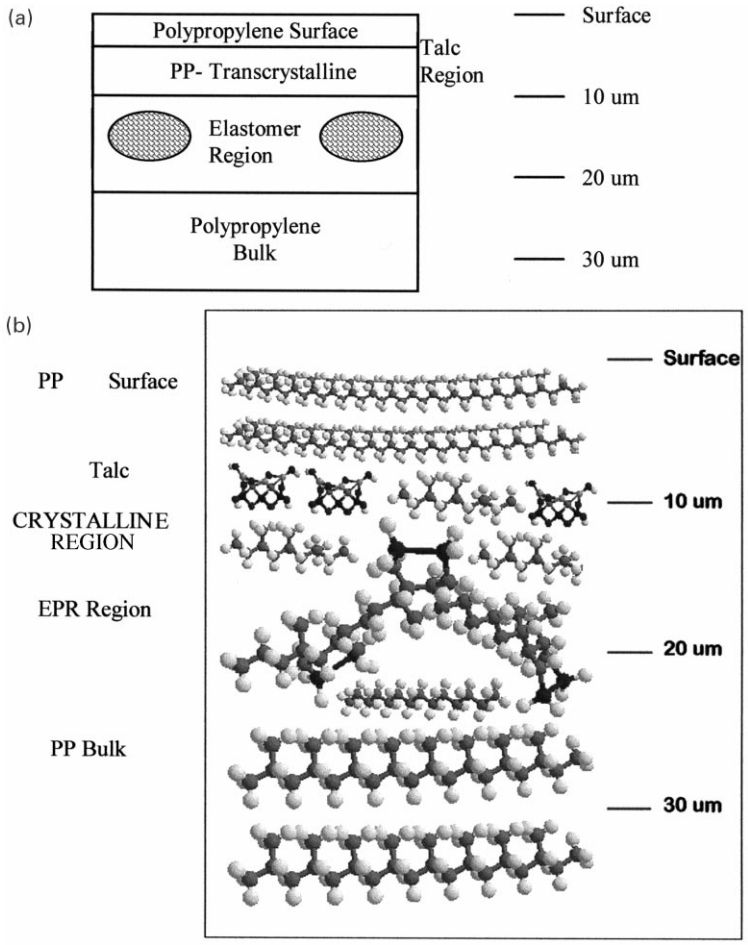

Fig. 8. (a) Side profile of proposed stratification profile of thermoplastic olefin (TPO). (b) Molecular level representation of thermoplastic olefin (TPO) stratification profile.

crystallite formation. Owing to the presence of irregularities and microscopic particles on the mold surface, nucleation of the polymer melt will result as heterogeneous crystallization occurs. As TPO is injection-molded, the relatively cooler surface of the mold will induce a crystallinity gradient in the polymer bulk. It was proposed that this process may lead to the formation of transcrystalline regions at the surface, as well as weak boundary layers (WBL) [47]. The formation of transcrystalline layers were shown by Ryntz to occur in the top 10 μm from the surface [22]. Below the ''skin'' layer, a second region results from high shearing conditions which produce a large number of row structures. As the temperature gradient is smaller in this region, the crystallite formation will be more organized. Additives, such as EPR, will tend to migrate to form higher concentration levels in this layer. A third region, lying below this high shear zone, will be less influenced by thermal conditions as a result of slower cooling rates. This will produce a polypropylene-rich layer with large spherulitic structures with no defined orientation present [48,49]. As a result of these gradient forces, the overall structure of EPR/PP blends will consist of a surface layer containing hard domains of PP at the surface of the mold, an intermediate soft EPR-rich region, and a polypropylene core near the center [18]. The model presented in Fig. 8a and deduced from PA FT-IR analysis agrees with the previous studies, and a nondestructive nature of photoacoustic measurements makes the analysis more reliable.

Based on literature and the photoacoustic data, we are in a position to propose a model of stratification for injection molded TPO. The surface of TPO contains PP layers which result from heterogeneous nucleation occurring during the molding process. The talc component distribution is high near the surface of TPO, which is associated with the PP crystallites. At 7–9 μm below the surface is the primary crystalline PP region, while elastomer rubber is found to be preferentially deeper in the bulk, at approximately 15 μm below the surface. While Fig. 8a illustrates a stratification model for TPO, Fig. 8b shows molecular representation of the stratification profile.

4. Conclusions

Using linear PA FT-IR depth profiling, individual component distributions of crystalline PP, EPR, and talc in injection molded TPO was determined. Using modulation

frequencies of $1.9\bar{\nu}$ to $0.032\bar{\nu}$ Hz in the 1500–600 cm^{-1} region, talc was predominantly detected at 5–7 μm below the surface, while the crystalline PP is detected at approximately 7–9 μm below the surface, and the EPR layer is at 15 μm and extends into the bulk. Based on the surface depth profiling experiments, DMTA analysis, and a component ratio curve, these studies indicate that the phase separation occurs across the film thickness, and the results obtained using DMTA confirm these findings. However, it should be kept in mind that the majority of phase separation phenomena occurs near surfaces or interfaces as they exhibit an excess of surface energy, and the use of DMTA may not adequately represent the actual situation.

Acknowledgements

The authors are thankful to the National Science Foundation Industry/University Cooperative Research Center in Coatings at North Dakota State University and Eastern Michigan University for financial support of these studies.

References

[1] Ramamurthy AC, Ryntz RA, Holubka JW, Hartmann B. Polym Mater Sci Eng 1992;69:28.
[2] Hirayama T, Urban MW. Prog Org Coat 1992;20:81.
[3] Salazar-Rojas EM, Urban MW. Prog Org Coat 1989;16:371–386.
[4] Ludwig BW, Urban MW. J Coat Technol 1994;66:59.
[5] Ludwig BW, Urban MW. J Coat Technol 1996;68:93.
[6] Kaminski, A.M., Urban, M.W., J Coat Technol, 1997 (submitted).
[7] Urban MW, Evanson KW. Polym Commun 1990;31:279.
[8] Evanson KW, Urban MW. J Appl Polym Sci 1991;42:2287.
[9] Evanson KW, Urban MW. J Appl Polym Sci 1991;42:2297.
[10] Niu BJ, Urban MW. J Appl Polym Sci 1995;56:377.
[11] Zhao CL, Holl Y, Pith T, Lambla M. Coll Polym Sci 1987;265:823.
[12] Thorstenson TA, Evanson KW, Urban MW. Polym Mater Sci Eng 1991;64:195.
[13] Evanson KW, Urban MW. J Appl Polym Sci 1991;42:2309.
[14] Thorstenson TA, Urban MW. J Appl Polym Sci 1993;47:1381.
[15] Thorstenson TA, Urban MW. J Appl Polym Sci 1993;47:1387.
[16] Niu BJ, Urban MW. J Appl Polym Sci 1996;60:389.
[17] Niu BJ, Urban MW. J Appl Polym Sci 1996;62:1903.
[18] Coleman PB, Carter RO. ANTEC 1995;x:1783.
[19] Clark ES. Appl Poly Symp 1974;24:45.
[20] Fitchmun DR, Mencik ZJ. Poly Sci: Poly Phys 1973;11:951.
[21] Bowman J, Harris N, Bevis MJ. J Materials Sci 1975;10:63.
[22] Ryntz RA. Prog Org Coat 1996;27:241.
[23] Fitchmun DR, Newman S, Wiggle R. J Appl Polym Sci 1970;14:2441.
[24] Schonhorn HJ. Polym Sci B 1965;2:185.
[25] Pukansky B, Tudos F, Kallo A, Bodor G. Polymer 1989;30:1399.
[26] Chatzi EG, Urban MW, Ishida H, Koenig JL. Polymer 1986;27:1850.
[27] Urban MW, Koenig JL. Appl Spectrosc 1986;40:994.
[28] Griffiths PR. Transform Techniques in Chemistry. New York: Plenum, 1978 p. 122.
[29] Griffiths PR, DeHaseth JA. Fourier Transform Infrared Spectrometry. Chemical Analysis Series, 83. New York: Wiley, 1900 p. 43.
[30] Rosencwaig A. Photoacoustics and Photoacoustic Spectroscopy. New York: John Wiley and Sons, 1980.
[31] Dittmar RM, Palmer RA. App Spec Rev 1994;29:171.
[32] Stagge J. Urban, MW. The 13th European Symp Polym Spectrosc, Lancaster, United Kingdom, 20–23 July, 1998.
[33] Miyazawa T, Fukushima K, Ideguchi Y. J Poly Sci Part B 1963;1:385.
[34] Tadokoro H, Kobayashi M, Ukita M. J Chem Phys 1965;42:1432.
[35] Kausch HH, Hassell JA, editors. Deformation and Fracture of High Polymers New York: Plenum, 1973.
[36] Vincent PI. Polymer 1974;15:111.
[37] Chu AP, Tebelius LK, Urban MW. In: Glass JE, editor. Technology for Waterborne Coatings, *ACS Symposium Series*, 663. Washington, DC: American Chemical Society, 1997 Chapter 12.
[38] Mishra V, Sperling LH. J Polym Mat 1996;13:93.
[39] Polymer Handbook; Brandrup J, Immergut EH, Eds.; Wiley: New York, 1989.
[40] De SK, Bhowmick AK, editors. Thermoplastic Elastomers from Rubber–Plastic Blends New York: Ellis Horwood, 1990.
[41] Singhal A, Fina LJ. Polymer 1996;37:2335.
[42] Ryntz RA, Xie Q, Ramamurthy AC. Ann. Waterborne, Higher-Solids and Powder Coating Symp, 11 Feb. 1994, New Orleans, LA.
[43] Pennings AJ, van der Mark AJ, Keil AM. Kolloid Z Z Polym 1970;237:336.
[44] Fitchmun DR, Newman S, Wiggle RJ. Appl Polym Sci 1970;14:2457.
[45] Kantz MR, Newman HD, Stigale FH. J Appl Polym Sci 1972;16:1249.
[46] Mencik Z, Fitchmun DR. J Polym Sci: Polym Phys 1973;11:973.
[47] Wu S, editor. Polymer Interface and Adhesion New York: Marcel Dekker, 1982.
[48] Sharples A. Introduction to Polymer Crystallization. New York: St. Martin, 1966 p. 5–24.
[49] Geil PH. Polymer Single Crystals. New York-London: Interscience, 1963 p. 223–304.
[50] Zerbi G, Piseri L. J Chem Phys 1968;49:3840.
[51] Peraldo M. Gazz Chim Ital 1959;89:798.